Journal of Marine Systems xxx (2011) xxx–xxx

Contents lists available at SciVerse ScienceDirect

Journal of Marine Systems

journal homepage: www.elsevier.com/locate/jmarsys

Modeling seasonal and diurnal pCO_2 variations in the northern South China Sea

Zhongming Lu [a,*], Jianping Gan [a], Minhan Dai [b]

[a] Division of Environment, Department of Mathematics, Hong Kong University of Science and Technology, Kowloon, Hong Kong, China
[b] State Key Laboratory of Marine Environmental Science, Xiamen University, Xiamen, China

ARTICLE INFO

Article history:
Received 12 April 2011
Received in revised form 30 September 2011
Accepted 3 October 2011
Available online xxxx

Keywords:
Carbon dioxide
Temporal variations
Air–water exchanges
Control factor
Modeling
South China Sea

ABSTRACT

This paper describes the simulated temporal variation of surface seawater CO_2 partial pressure (pCO_2) in the northern South China Sea. We produced the simulations with a one-dimensional (1-D) coupled physical–biogeochemical model that had high-frequency, time-dependent atmospheric forcing and that were validated with field observations. We also examined the associated processes that modulate seawater pCO_2 at different time scales, from diurnal to seasonal, using a series of process-oriented experiments. At seasonal time scales, we revealed that the sea–air CO_2 exchange was a primary process that modulated surface pCO_2 and exceeded the role of sea surface temperature (SST) even though the phase of the pCO_2 variation generally followed the strong seasonal cycle of SST. This was because sea–air CO_2 exchange is a slow process and has an accumulative effect on surface water pCO_2 due to the buffering effect of the carbonate system once CO_2 has dissolved in the seawater, which leads to a long equilibration time of CO_2 between the atmosphere and seawater. The mixing effect on pCO_2 induced by total alkalinity and dissolved inorganic carbon variations was, generally, positively correlated with the seasonal evolution of wind speed. Biological processes were the smallest contributors to pCO_2 variations at the seasonal scale because of the oligotrophic characteristic of the region. At diurnal time scales, the dominant pCO_2 controlling factor was mainly associated with the local physical and biological conditions. Temperature and wind-induced vertical mixing played major roles in pCO_2 when the winter heat flux and upward transport of low temperature and high pCO_2 in deep water were intensified. Phytoplankton blooms generally occur after a period of strong wind, as a result, biological metabolism becomes the most important pCO_2 regulator when the surface chlorophyll-a reached its highest level. Unlike that in the seasonal scale, the effect of sea–air CO_2 exchange was minor at diurnal time scales due to the long equilibration time of CO_2 between the atmosphere and seawater. We also found that the frequency of the model driving force was important in reproducing the sea surface pCO_2. The high frequency forcing was important in controlling the pCO_2 variation through the feedback effect to the corresponding physical and biogeochemical responses.

1. Introduction

It is known that the ocean has been a major sink for anthropogenic CO_2 (Falkowski et al., 2000), and its capacity to uptake atmospheric CO_2 can be manifested by the difference in the partial pressure of CO_2 (pCO_2) between the air and ocean surface. While pCO_2 in the atmosphere is largely homogeneous due to relatively rapid atmospheric circulation, the surface seawater pCO_2 field varies greatly in time and space. This variability drives the CO_2 source or sink traits of a particular oceanic region and has received great attention during the past 10 years (Takahashi et al., 2009).

pCO_2 in seawater is generally modulated by both physical and biogeochemical processes such as mixing with different water masses, temperature changes, chemical buffering, sea–air exchange, and biological metabolic activities (Murnane et al., 1999; Zhai and Dai, 2009). There have been many attempts (Cai et al., 2006; Takahashi et al., 2009), primarily based on ship-board observations, to obtain a mechanistic understanding of the CO_2 variability in order to improve our knowledge of CO_2 behavior within a specific system and to generalize to global scales ultimately to acquire a predictive capacity. The current challenge is to differentiate the fractional influences of the different sources that modulate the CO_2 variations based on the analysis on an integrated understanding of the coupled physical–biogeochemical processes in time and space (McKinley et al., 2006; Previdi et al., 2009). Such attempts are compounded by the fact that CO_2 variability may be dominated by different controls at different time scales which have not been well-understood thus far (Bates et al., 1998; Dai et al., 2009). For this purpose, numerical simulations of coupled physical–biogeochemical processes, combined with *in situ* observations, necessarily provide a dynamic interpolation or extrapolation of incomplete measurements and compensate for the temporal and spatial limitations of field CO_2 measurements (Fujii et al., 2009).

* Corresponding author. Tel.: +852 23588431; fax: +852 23581582.
E-mail address: luzm@ust.hk (Z. Lu).

0924-7963/$ – see front matter © 2011 Elsevier B.V. All rights reserved.
doi:10.1016/j.jmarsys.2011.10.003

More importantly, the examinations are performed through process-oriented numerical experiments that can identify intrinsic controlling mechanisms of pCO_2.

The South China Sea (SCS) is the second largest marginal sea in the world. Driven by the strong Asian monsoon, it is characterized by diverse spatio-temporal physical and biological dynamics, and it plays an important role in regional climate variability (Liu et al., 2002). Using their observed pCO_2 data from three cruises that were conducted in the spring, summer, and late fall, Zhai et al. (2005, 2007) reported a pCO_2 variation range of 360 to 450 μatm, and suggested that the northern SCS (NSCS) was a weak/moderate CO_2 source (~0.86 mol m^{-2} $year^{-1}$) for the atmosphere on an annual basis.

To investigate the carbon cycle controlling mechanisms and to study the effect of interactions between the upper ocean and the sea surface atmosphere on the biogeochemical processes in the NSCS, the South East Asia Time Series Study established a station (the SEATS station) that is located at the edge of the continental margin close to the deep basin in the NSCS (116°E, 18°N) in 1999, and observed onsite every 2–4 months (Wong et al., 2007). Chou et al. (2005) found that the fCO_2 (fugacity of CO_2) reached a minimum of 347 μatm in winter and a maximum of 382 μatm in summer by using bimonthly pCO_2 data collected from March 2002 to April 2003 at SEATS. Unlike Zhai et al., (2005), they identified that the annual sea–air CO_2 flux was a weak sink to the atmosphere (−0.11 to −0.23 mol C m^{-2} yr^{-1}). Subsequently, Tseng et al. (2007) reported an intra-annual fluctuation of pCO_2 between 340 and 400 μatm and a nearly zero sea–air flux of 0.02 mol C m^{-2} yr^{-1}. These previous observation-based studies pointed out that the temperature effect overwhelms biological forcing and is the major controlling factor of surface water pCO_2.

Based on a three-dimensional coupled physical–biogeochemical model, Chai et al. (2009) simulated the physical variation, ecosystem response, and carbon cycle in the SCS basin. They pointed out that SST has a greater influence than biological forcing, and is the dominant controlling factor on surface seawater pCO_2 through an empirical estimation given by Takahashi et al. (2002). They also found that total alkalinity (TA) and dissolved inorganic carbon (DIC) have less influence on pCO_2 than SST based on their sensitivity experiments.

We contend, however, that to resolve the CO_2 dynamics in a complex system like the SCS, studies performed solely with qualitative evaluations derived from spatially and temporally limited field measurements are not enough. We also contend that temporal variations and the intrinsic controls are subject to spatial variations, and should be examined on an individual spatial domain basis. A continuously stratified vertical 1-D coupled physical–biogeochemical model with high-frequency, time-dependent atmospheric forcing would effectively identify the fundamental controlling processes of pCO_2 at different time scales. We selected the SEATS stations to start our modeling efforts because time series observational data have been available at this station since 1999. Furthermore, we only used a 1-D model to emphasize the determination of CO_2 dynamics on different time scales.

The organization of this paper is as follows. The study methods, including a brief description of the 1-D model framework, model setup, and observational data are introduced in Section 2. Section 3 mainly focuses on comparison between model results and observational data. In Section 4, we analysis different processes that modulate seawater pCO_2 at seasonal and diurnal time scales, and the role of driving force frequency in the model is also discussed. A summarization of the results obtained in this study is presented in Section 5.

2. Methods

2.1. Model description

The 1-D model is an implementation of the Regional Ocean Modeling System (ROMS, http://www.myroms.org) (Haidvogel et al., 2008; Shchepetkin and McWilliams, 2005) coupled with the Fasham-type ecosystem model (Fasham et al., 1990). We applied the model to the SEATS station data (Fig. 1). Hydrodynamics of the model are governed by the primitive equations and a local closure scheme that is based on level-2.5 turbulent kinetic energy equations (Mellor and Yamada, 1982) and that is adopted in the vertical mixing parameterization. In our application, the domain was centered at 18°N, 116°E with a water depth of 3770 m. The model has 60 vertical levels with vertically variable grid-spacing. To better resolve the surface boundary layer, we adopted a grid-spacing of about 5 m in the upper layer, and spacing was about 60 m and 130 m in the bottom and middle layers, respectively. The model time step is 800 s.

The ecosystem module was embedded in the ROMS (Fennel et al., 2006). It is a nitrogen-based ecosystem model that includes 7 prognostic variables: nitrate (NO_3, N), ammonium (NH_4, A), Chlorophyll-*a* (Chla), phytoplankton (P), zooplankton (Z), large detritus (LD), and small detritus (SD). The details of the model were described in Gan et al. (2010) and Lu et al. (2010), both of who successfully simulated the dynamics of the biological response to coastal upwelling and a river plume over the shelf of the NSCS.

The carbonate system module was also embedded in the ROMS. The surface seawater pCO_2 depends on salinity, SST, TA, and DIC. TA and DIC are altered by biological processes as well as by physical mixing. The calculation of the surface seawater pCO_2 follows Zeebe and Wolf-Gladrow (2005). The equations governing TA and DIC in seawater are:

$$\frac{\partial [TA]}{\partial t} = \left(\frac{\partial [TA]}{\partial t}\right)_M + \left(\frac{\partial [TA]}{\partial t}\right)_B \tag{1}$$

$$\frac{\partial [DIC]}{\partial t} = \left(\frac{\partial [DIC]}{\partial t}\right)_M + \left(\frac{\partial [DIC]}{\partial t}\right)_F + \left(\frac{\partial [DIC]}{\partial t}\right)_B \tag{2}$$

$$\left(\frac{\partial [TA]}{\partial t}\right)_B = \left(\frac{\partial [TA]}{\partial t}\right)_{NP} - \left(\frac{\partial [TA]}{\partial t}\right)_{Nitri} \tag{3}$$

$$\left(\frac{\partial [TA]}{\partial t}\right)_{NP} = t_{PP\max} \cdot \frac{K_N \cdot [N] \cdot [P]}{(1 + K_A \cdot [A]) \cdot (1 + K_N \cdot [N])} \tag{4}$$

$$\left(\frac{\partial [TA]}{\partial t}\right)_{Nitri} = [A] \cdot n_{\max} \cdot \left(1 - \max\left(0, \frac{PAR - I_0}{K_I + PAR - 2 * I_0}\right)\right) \tag{5}$$

$$PAR_k = PAR_{k+1} \cdot e^{-0.5 \cdot \left(k_{water} + k_{Chla} \cdot [Chla]_k\right) \cdot \Delta z_k} \tag{6}$$

$$\left(\frac{\partial [DIC]}{\partial t}\right)_B = \left(\frac{\partial [DIC]}{\partial t}\right)_P + \left(\frac{\partial [DIC]}{\partial t}\right)_Z + \left(\frac{\partial [DIC]}{\partial t}\right)_R \tag{7}$$

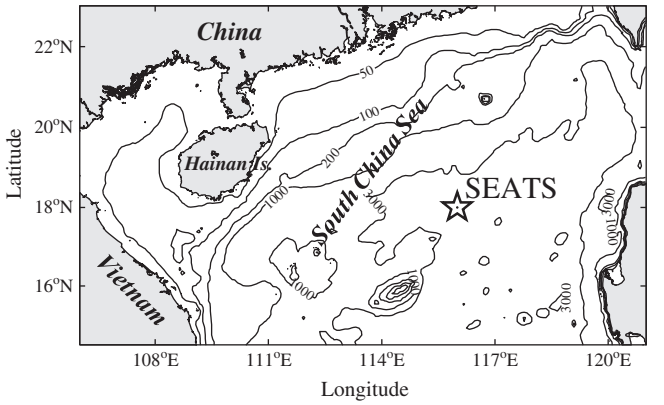

Fig. 1. Map with isobaths of the northern South China Sea showing the major study site (SEATS) as a pentagram.

Please cite this article as: Lu, Z., et al., Modeling seasonal and diurnal pCO_2 variations in the northern South China Sea, J. Mar. Syst. (2011), doi:10.1016/j.jmarsys.2011.10.003

$$\left(\frac{\partial[DIC]}{\partial t}\right)_P = -r_{C:N,P}\cdot\left(t_{PP\max}\cdot\frac{K_N\cdot[N]\cdot[P]}{(1+[A]\cdot K_A)\cdot(1+[N]\cdot K_N)}+t_{PP\max}\cdot\frac{K_A\cdot[A]\cdot[P]}{1+[A]\cdot K_A}\right) \quad (8)$$

$$\left(\frac{\partial[DIC]}{\partial t}\right)_Z = r_{C:N,Z}\cdot\left(l_{BM}\cdot\max([Z]-Zoo_{Min},0)+\frac{L_E\cdot[P]^2}{K_P+[P]^2}\cdot AE_N\cdot[Z]\right) \quad (9)$$

$$\left(\frac{\partial[DIC]}{\partial t}\right)_R = [SD]\cdot r_{SD}+[LD]\cdot r_{LD} \quad (10)$$

$$t_{PP\max} = \frac{\mu_{\max}\cdot PAR\cdot\alpha}{\sqrt{\mu_{\max}{}^2+PAR^2\cdot\alpha^2}} \quad (11)$$

where M represents mixing (advection + diffusion); F and B represent sea–air flux and the biological process, respectively; NP refers to new production; $Nitri$, P, and Z represent nitrification, phytoplankton photosynthesis, and zooplankton basal metabolism and excretion, respectively; PAR represents photosynthetic active radiation; R is detritus remineralization; $\mu_{\max}$ is the maximum growth rate of phytoplankton, and $t_{PP\max}$ is the rate of maximum primary productivity.

The sea–air CO_2 flux of (F_{CO2}) was calculated by:

$$F_{CO_2} = k\cdot K_H\cdot\Delta pCO_2, \quad (12)$$

where k is the gas transfer velocity; K_H is the solubility of CO_2 in seawater (Weiss, 1974); and ΔpCO_2 is the difference between the pCO_2 in the surface seawater and in the overlying air. The gas transfer velocity, k, was calculated from wind speed under steady wind conditions according to Wanninkhof (1992):

$$k = 0.31\cdot u^2\cdot\left(\frac{Sc}{660}\right)^{-\frac{1}{2}} \quad (13)$$

where u is the wind speed at 10 m above sea level calculated from wind stress and Sc is the Schmidt number for CO_2 (which is a function of SST).

A schematic diagram of the biological and carbon cycle module is shown in Fig. 2. The related parameters of the model are listed in Table 1. The biological and carbon cycle module were coupled with the physical module at identical temporal and spatial resolutions. Since some differences existed in the environmental settings and functions between the original model and this application, necessary modifications of the calculation of total alkalinity, CO_2 solubility, and CO_2 sea–air flux were made in the model. The details are presented in the Appendix.

2.2. Model setup and data

Seawater salinity, temperature, TA, DIC, NO_3, and Chla were derived from field observations at SEATS (http://www.ncor.ntu.edu.tw/SEATS/Data%20Links/) (Tseng et al., 2007). In the initial stage of the SEATS project (September 1999 to July 2000), sampling frequency was bimonthly and then changed to seasonally. Data from the initial sampling stage were used for model validation in our study.

We first performed a spin-up with field data from March 1999 that included salinity, temperature, TA, DIC, NO_3, and Chla (http://140.112.65.17/odbs/seats/index.htm). Initial phytoplankton, zooplankton, and detritus were derived from Chla data assuming a ratio of 1.59 and 0.70 for Chla/phytoplankton, and detritus/phytoplankton, respectively (Evans and Garcon, 1997). During spin-up, the model was forced with monthly-averaged wind stress and heat flux from April 1999 to March 2000 derived from the National Centers for Environmental Prediction (NCEP, http://www.ncep.noaa.gov/). The atmospheric pCO_2 was set to a constant value of 370 µatm. The model was spun up for 5 years (5 cycles of April 1999 to March 2000). The averages of all biological variables (NO_3, Chla, phytoplankton, zooplankton, and detritus) in month 60 of the spin-up run were exported as the initial biological conditions of the real-time simulation.

After initialization the model was forced with six-hourly wind stress, net short wave radiation flux, evaporation–precipitation (E–P), air temperature, relative humidity, air pressure, and total cloud cover using NCEP data from April 1999 to October 2000 (Fig. 3). The seasonal variation of atmospheric pCO_2 was determined by fitting the observations from the NSCS (Zhai et al., 2005) to the variation trend observed at the Mauna Loa Observatory (Keeling, 2008), with a minimum of ~364.5 µatm in August and a maximum of ~372.5 µatm in April. A weak SST nudging was applied for the seasonal scale simulation.

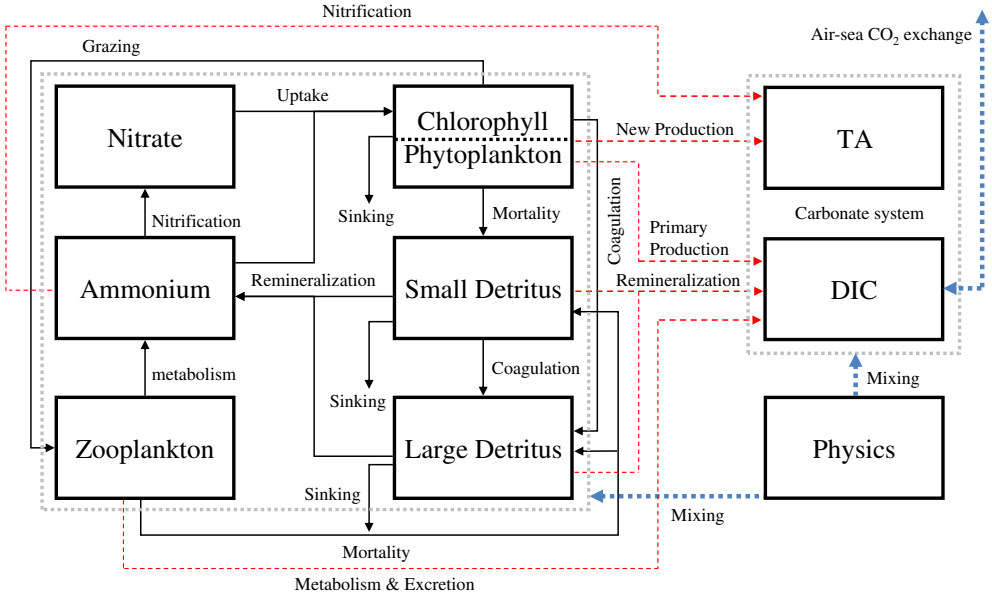

Fig. 2. Schematic diagram of the coupled physical–biogeochemical model. Boxes enclosed by the gray dotted line on the left side represent the biological variables of the model. The black solid lines with arrows indicate the biological processes between different biological variables. Boxes enclosed by the gray dotted line on the right side represent chemical variables which directly determine the pCO_2. The red dashed lines with arrows show the biological processes affecting the carbonate system in the seawater. Blue dotted lines with arrows indicate the physical processes affecting the biogeochemical variables. (For interpretation of the references to color in this figure legend, the reader is referred to the web version of this article.)

Please cite this article as: Lu, Z., et al., Modeling seasonal and diurnal pCO_2 variations in the northern South China Sea, J. Mar. Syst. (2011), doi:10.1016/j.jmarsys.2011.10.003

Table 1
Biogeochemical model parameters.

Description	Symbol	Value	Units
Light attenuation due to seawater	k_{water}	0.04[a]	m^{-1}
Light attenuation by Chla	k_{Chla}	0.025[a]	$(m^2\ mg\ Chla)^{-1}$
Initial slope of the P–I curve	α	0.025[a]	mg C (mg Chla W m^{-2} d)$^{-1}$
Half-saturation for phytoplankton NO_3 uptake	K_N	0.5[b]	mmol N m^{-3}
Half-saturation for phytoplankton NH_4 uptake	K_A	0.5[b]	mmol N m^{-3}
Zooplankton assimilation efficiency for nitrogen	AE_N	0.75[b]	–
Zooplankton half-saturation constant for ingestion	K_P	1[b]	mmol N m^{-3}
Zooplankton minimum threshold value	Zoo_{Min}	0.001[c]	mmol N m^{-3}
Zooplankton basal metabolism	l_{BM}	0.1[b]	d^{-1}
Zooplankton specific excretion rate	L_E	0.1[b]	d^{-1}
Phytoplankton carbon to nitrogen ratio	$r_{C:N,P}$	6.625[d]	mol C (mol N)$^{-1}$
Zooplankton carbon to nitrogen ratio	$r_{C:N,Z}$	6.625[d]	mol C (mol N)$^{-1}$
Small detritus remineralization rate	r_{SD}	0.03[b]	d^{-1}
Large detritus remineralization rate	r_{LD}	0.01[b]	d^{-1}
Maximum nitrification rate	n_{max}	0.05[b]	d^{-1}
Threshold PAR for nitrification inhibition	I_0	0.0095[b]	W m^{-2}
Half-saturation PAR for nitrification inhibition	k_I	0.1[c]	W m^{-2}

[a] Fasham et al. (1990).
[b] Fennel et al. (2006).
[c] Model default value.
[d] Redfield (1958).

3. Results

3.1. Model-observation comparison

The variation of surface water pCO_2 is a composite process simultaneously affected or controlled by multiple factors. The model was first evaluated by conducting a model-observation comparison. Fig. 4 shows the simulated salinity, temperature, TA, DIC, and NO_3 profiles from the whole water column and for the top 200 m in summer and winter, respectively. Also shown in Fig. 4 are the corresponding profiles of the observations. Generally, there was very good agreement between modeled and observed data for the entire water column, especially in the upper 50 m (Fig. 4a, b). The exception was the simulated salinity in the upper layer, where the modeled surface salinity was lower than the observed one. This was probably due to the generally negative E–P in this region (Fig. 3, also see (Swapna et al., 2009)) and the fact that the advective effects from ocean currents could not be resolved in this 1-D simulation. Nevertheless, the generally good agreement between model and observations indicated that the model captured the characterized response to the internal biological processes and external forcing reasonably well. The validated model provided a solid basis for the mechanism analysis of the carbon cycle.

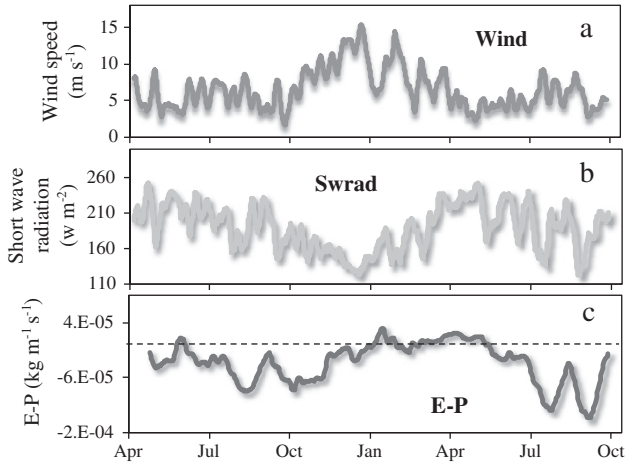

Fig. 3. Time series of six-hourly (a) wind speed (m s^{-1}), (b) short wave radiation (Wm^{-2}), and (c) evaporation minus precipitation (E–P) (kg m^{-2} s^{-1}) from Apr 1999 to Oct 2000. The dashed line in (c) is the zero line. Data were derived from National Centers for Environmental Prediction (http://www.ncep.noaa.gov/).

Fig. 5 shows the seasonal variations of monthly temperature, DIC, and NO_3 in SEATS from September 1999–July 2000. The observations in the figure are reproduced from the results published on the SEATS web page (http://www.ncor.ntu.edu.tw/SEATS/Data Links/). Both the observed data and simulated results showed significant seasonal variations. The temperature time series clearly indicates that the water column remained highly stratified in the summer and was strongly mixed in the winter (Fig. 5a, d). DIC shows a similar pattern of seasonal variations with relatively low values during spring, summer, and autumn when the water column was well-stratified. In the winter (December to February), as the northeastern monsoon strengthened, subsurface waters with high DIC mixed upwards to the surface (Fig. 5b, e). However, different from temperature and DIC, there was no obvious upward intrusion of NO_3 in the upper layer in the observed or the simulated fields in the winter, which indicated the likelihood of a strong biological uptake due to the annual maximum of winter primary production in the region (Tseng et al., 2005). Actually, there do have very weak upward intrusion of NO_3 (~0.25 μmol L^{-1}) during winter, although it is very hard to distinguish from background. Our sensitivity experiment (not shown) also showed stronger increase of NO_3 in the surface layer during the winter when there was no biological forcing.

The ammonium is also an important indicator of the biological activities since the regenerated production (utilizing NH_4) is more significant than the new production (utilizing NO_3) in this region. In this model, both the new production and the regenerated production were considered as important components that regulate the seawater carbonate system as reflected by Eqs. (4) and (8). However, NO_3 is still the most commonly used parameter to indicate the biological activities because there is still no solid observational data of NH_4 in this region to date. On the other hand, according to the existing studies, the f-ratio (integrated new production (INP)/integrated primary production (IPP)) has significant seasonal variability that coincidentally varied with the concentration of NO_3 (Chen, 2005). The model results also showed that the seasonal variation of NH_4 in the surface water was relatively stable, while NO_3 varies from near zero during spring, summer and autumn to about 0.25 μmol L^{-1} in winter. This suggests, although the regenerated production based on NH_4 contributes more to primary production, the new production based on NO_3 may be still the better parameter to indicate the variation of biological processes.

The simulated time series of depth integrated Chla (Fig. 6) also agreed well with observations. Significant seasonal variations occurred during the simulated period. Stimulated by nutrients from the deep layer, due to strengthened wind-driven vertical mixing and upwelling by a local eddy, the strongest Chla increase was observed in the winter (December to February). The local eddy was identified from AVISO (Archiving, Validation and Interpretation of Satellite Oceanographic data, http://www.aviso.oceanobs.com/duacs/) daily absolute geostrophic currents. The two Chla centers, which coincided with the two peaks of wind speed in December and January (Fig. 3a), were captured in the simulation with high-frequency atmospheric forcing but were absent in the lower frequency measurements.

3.2. Seasonal variation of surface water pCO_2 and sea–air CO_2 flux

According to current understanding, the surface water pCO_2 of the NSCS has a clear seasonal cycle that is mainly controlled by variations

Please cite this article as: Lu, Z., et al., Modeling seasonal and diurnal pCO_2 variations in the northern South China Sea, J. Mar. Syst. (2011), doi:10.1016/j.jmarsys.2011.10.003

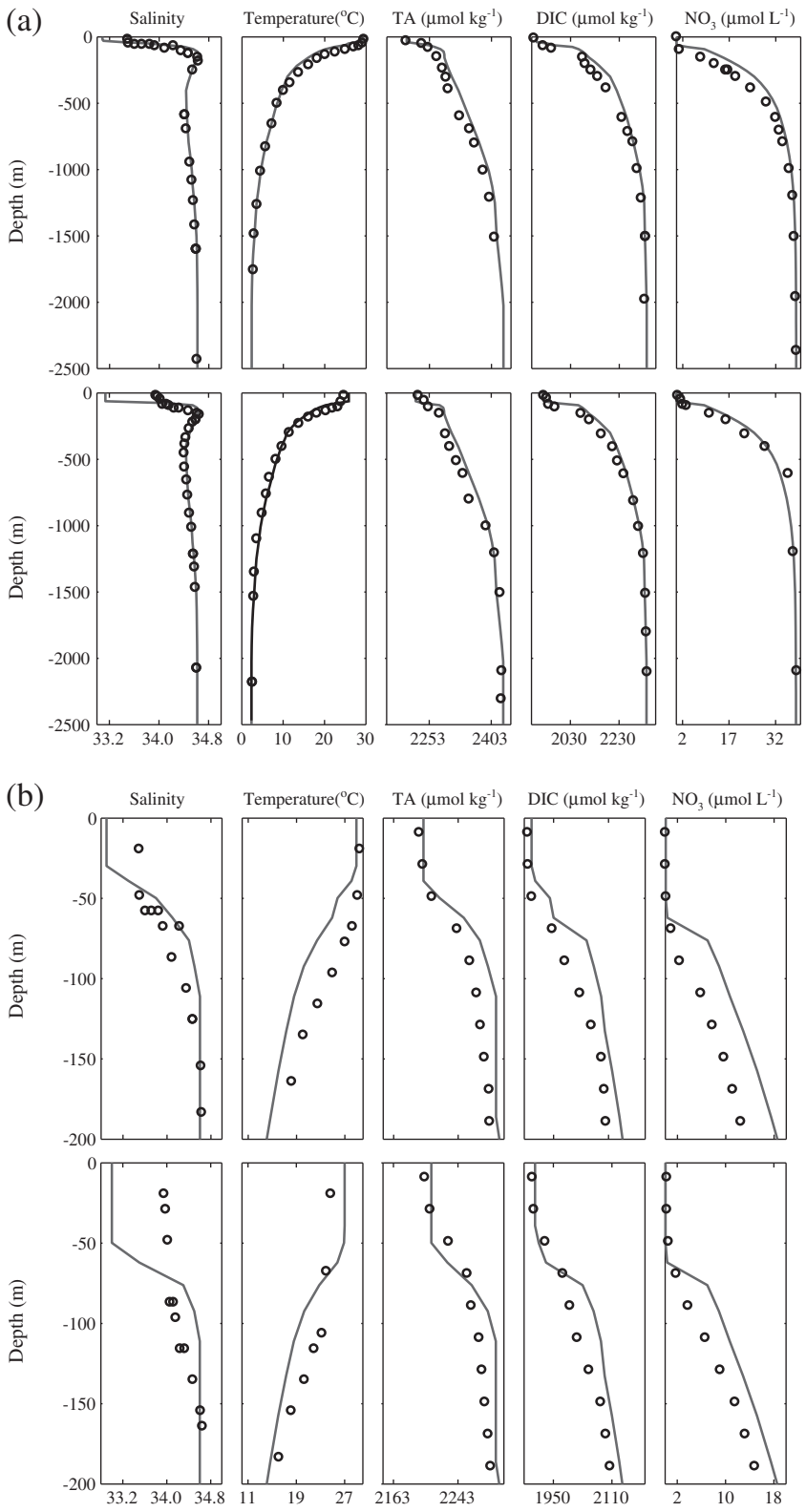

Fig. 4. Comparison between observed (open circle) and modeled (solid line) profiles of (a) the whole water column and (b) the top 200 m, in summer (upper panel) and winter (lower panel), respectively. The observed data were derived from the SEATS web page (http://www.ncor.ntu.edu.tw/SEATS/Data Links/) and Tseng et al. (2007).

in temperature. The NSCS either plays the role of a weak CO_2 sink or that of a source for the atmosphere (Chou et al., 2005; Tseng et al., 2007; Zhai et al., 2005). Fig. 7 shows that the simulated surface water pCO_2 varied in the range of ~350 μatm–410 μatm, on a seasonal scale, with the lowest value in winter (~January) and the highest value in summer (~June). In general, the simulated pCO_2 followed the variability in SST (Fig. 5d, Fig. 7). The overall magnitude of the simulated pCO_2 is about 10 μatm higher than observed pCO_2 (Chou et al., 2005; Zhai et al., 2005). One possible reason for the differences between our model and the observations was that uncertainties of the C/N ratio that converted the nitrogen to carbon in the model, while calculating the DIC, might have been altered by biological

Please cite this article as: Lu, Z., et al., Modeling seasonal and diurnal pCO_2 variations in the northern South China Sea, J. Mar. Syst. (2011), doi:10.1016/j.jmarsys.2011.10.003

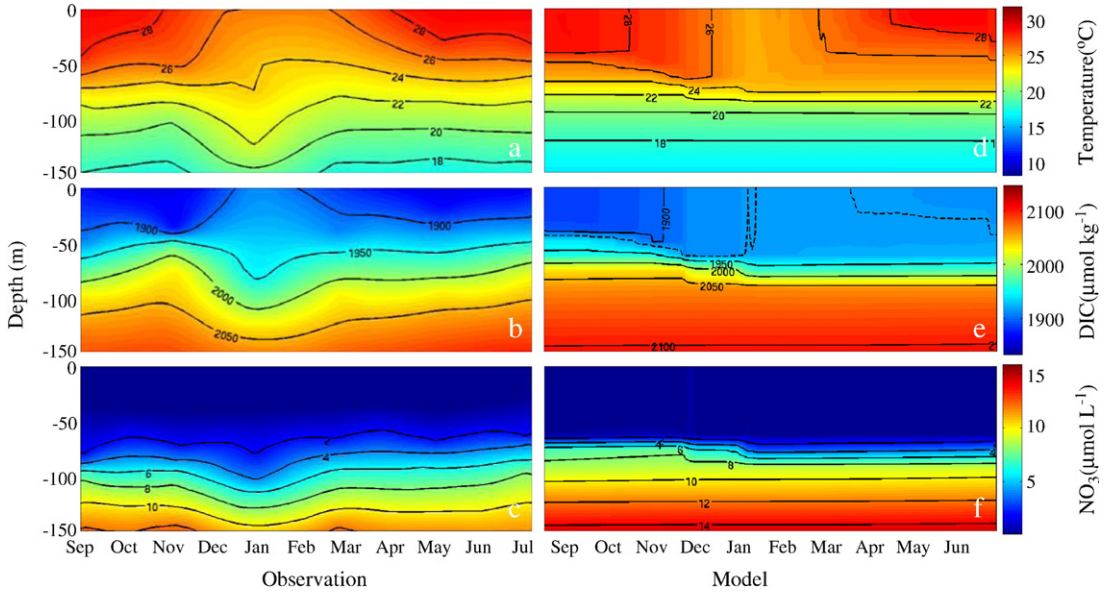

Fig. 5. Comparison between observed (left column) and modeled (right column) time series variation of temperature (a, d) (°C), DIC (b, e) (μmol kg^{-1}), and NO_3 (c, f) (μmol L^{-1}) in the upper 150 m water column between Sept. 1999 and Jul. 2000. The observations were reproduced from the figures available on the SEATS web page (http://www.ncor.ntu.edu.tw/SEATS/Data Links/).

metabolism (Eqs. (7)–(10)). The C/N ratio of phytoplankton and zooplankton used in this model was set to 6.625, according to the Redfield ratio (Redfield, 1958). However, the observed C/N ratios in the SEATS data ranged from 5.5 to 11.4 (Liu et al., 2007). Thus, if the C/N ratio in this region, or during the study period, happened to be higher than 6.625, the DIC consumption due to primary production would have been underestimated by the model. This would have led to a higher seawater pCO_2. Indeed, our sensitivity experiment (not shown) showed that an increase in the C/N ratio in the model resulted in a lower pCO_2. Another possible reason for the higher simulated pCO_2 was the absence of frequently occurring eddies and complex ocean currents in the model that could alter seawater carbonate chemistry. In this process-oriented 1-D study, the C/N ratio in the model was chosen as 6.625 to avoid complication or error.

According to Eq. (12), the seasonal cycle of CO_2 sea–air fluxes generally follows the evolution of surface seawater pCO_2, because the amplitude of seawater pCO_2 is about one order of magnitude larger than the atmospheric pCO_2 on a seasonal scale (~50 μatm of seawater pCO_2 and ~8 μatm of atmospheric pCO_2 respectively for this study). According to Eq. (13), wind speed is also an important parameter that determines the magnitude of sea–air CO_2 fluxes. By integrating the simulated sea–air flux from July 1999 to June 2000 (roughly the same period as when the bimonthly field observations at SEATS were performed), we obtained an annual sea–air CO_2 flux of 1.26 mmol C m^{-2} d^{-1} or 0.46 mol C m^{-2} yr^{-1}. Such a flux was higher than −0.11 to −0.23 mol C m^{-2} yr^{-1} that was reported by Chou et al. (2005) and the 0.02 mol C m^{-2} yr^{-1} reported by Tseng et al. (2007). Our result suggests that the NSCS, if represented by SEATS, was a weak source of CO_2 to the atmosphere. Nevertheless, both our model and the observations suggest that the NSCS was an insignificant source or sink for atmospheric CO_2.

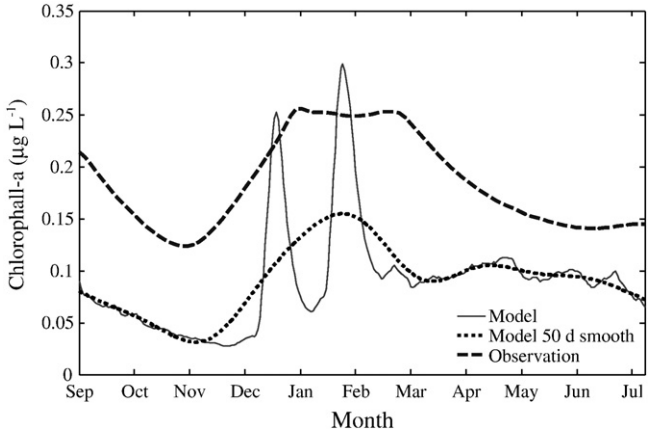

Fig. 6. The simulated evolution of depth averaged Chla concentration (solid line) and the 50 days smoothed result (dotted line, the 50-days' smoothing was made to remove the high frequency variation due to the high frequency atmospheric forcing and lacking horizontal advection in this 1-D simulation). The observations (dashed line) were reproduced from the figures available on the SEATS web page (http://www.ncor.ntu.edu.tw/SEATS/Data Links/).

4. Analysis and discussion

Surface seawater pCO_2 is affected by a suite of physical and biogeochemical processes including SST variations, vertical mixing, photosynthesis/respiration, calcium carbonate precipitation/dissolution, and sea–air CO_2 exchanges. In this section, the relative contribution of

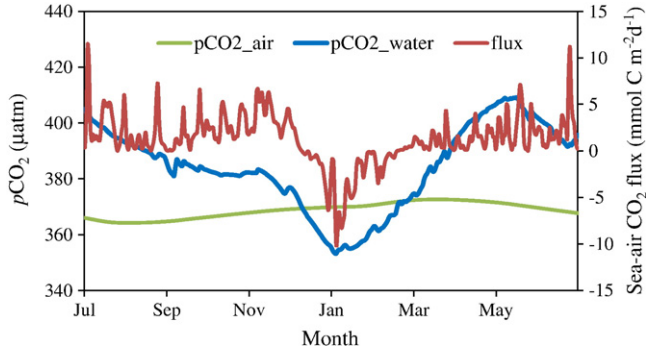

Fig. 7. Time series of observed atmospheric pCO_2, simulated sea surface pCO_2 and sea–air CO_2 flux from September 1999 to July 2000. The positive value of sea–air CO_2 flux indicates the CO_2 transfer from sea to air (the sea acts as a CO_2 source to atmosphere), the negative indicates the CO_2 transfer from air to sea (the sea acts as a CO_2 sink to atmosphere).

Please cite this article as: Lu, Z., et al., Modeling seasonal and diurnal pCO_2 variations in the northern South China Sea, J. Mar. Syst. (2011), doi:10.1016/j.jmarsys.2011.10.003

different factors and processes to pCO_2 variability on different time scales, and under different environmental conditions, is analyzed.

4.1. Controls of seasonal pCO_2 variability

Both the observed and simulated pCO_2 exhibited strong seasonality; most biogeochemical variables and the forcing also showed a significant seasonal cycle (Figs. 3 and 5). This indicated that the pCO_2 seasonal variation might have been co-regulated by various processes.

4.1.1. Role of SST

Seawater pCO_2 is positively correlated with temperature. To isolate the temperature effect from other forcing on pCO_2 variability, we turned off the sea–air CO_2 flux and ran two cases: with and without a fixed temperature in the surface water pCO_2 calculation. The fixed temperature was set to the mean temperature from August 1999 to July 2000. The pCO_2 difference between these two cases could be regarded as the net temperature effect (defined as pCO_{2T}). Thus, the pCO_2 without the temperature effect (defined as $NpCO_2$) could be calculated using Eq. (14):

$$NpCO_2 = pCO_2 \text{ at SST} - pCO_{2T} \quad (14)$$

Fig. 8a shows that the amplitude of the pCO_2 seasonal variation decreased from ~60 μatm (~350 μatm to ~410 μatm) in the standard case to ~30 μatm (~370 μatm to ~400 μatm)in the case with constant temperature. Because many other physical processes, such as vertical mixing and sea–air CO_2 exchange, might have also significantly contributed to the pCO_2 variation, it would have been erroneous to ignore these processes and treat the $NpCO_2$ as a net biological effect unless these processes became small or they offset each other (Takahashi et al., 2002).

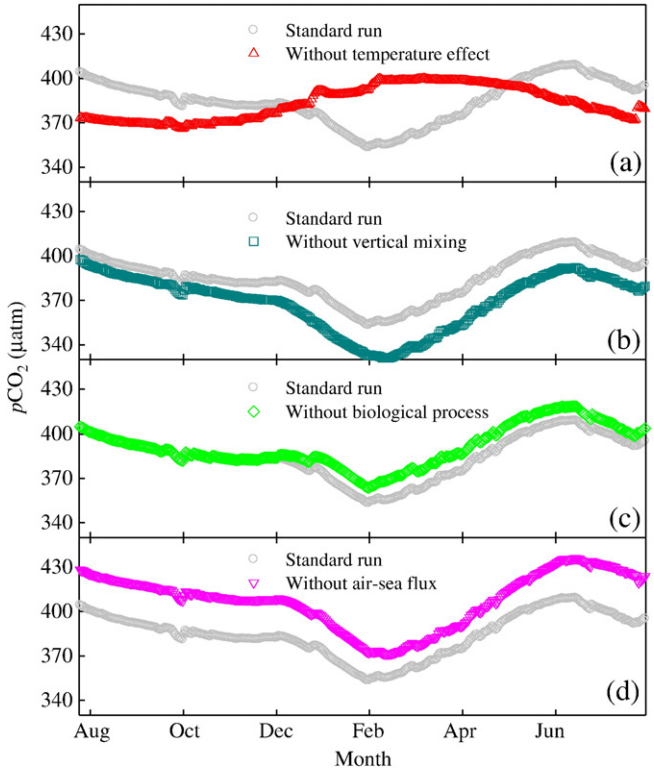

Fig. 8. pCO_2 variations without the effect of (a) temperature, (b) vertical mixing, (c) biological processes, and (d) sea–air flux, respectively (colored lines). The gray lines are the results from the standard run (with all effects). (For interpretation of the references to color in this figure legend, the reader is referred to the web version of this article.)

4.1.2. Mixing-induced chemical forcing

Vertical mixing brings the low temperature subsurface waters (with high TA, DIC, and nutrient concentration) into the surface layer. Nutrients have a relatively minor direct effect (the effect of chemical processes) on pCO_2, especially in an oligotrophic system (Louanchi et al., 1996). In addition, the indirect effect on pCO_2 caused by nutrients variation was ascribed to biological processes. We did not consider the direct effect of mixing-induced nutrient variation on pCO_2. Similarly, the SST variation due to mixing was hard to separate from that caused by air temperature. Thus, the mixing effect herein indicated the effect on pCO_2 induced solely by the TA and DIC variations. To examine the importance of mixing, their effects were removed by initializing the model with vertically uniform TA and DIC and with the surface layer concentration. Fig. 8b shows the comparison between the standard run and the case without vertical mixing. The pCO_2 in the case without vertical mixing was generally lower than that of the standard case, which indicated a high potential pCO_2 in the deeper layer (The potential pCO_2 is the pCO_2 of a parcel of seawater that would have under sea surface temperature and pressure).

Similarly, by subtracting the pCO_2 in the case from that in the standard case, we found that the net effect of vertical mixing on pCO_2 was always positive and ranged from 6 μatm to 24 μatm due to the higher potential pCO_2 in the deep layer (Fig. 9). The mixing effect reached its maximum in winter when the wind was strongest. The weakest mixing occurred from September to October during the monsoon transition period which was consistent with the seasonal evolution of wind speed (Fig. 3).

4.1.3. Biological forcing

In the marine ecosystem, phytoplankton regulates the seawater carbonate system through photosynthesis and respiration, zooplankton exert its influence on the pCO_2 variability through its metabolism directly or through its grazing on phytoplankton indirectly, since zooplankton grazing is an important source of phytoplankton mortality (Liu et al., 2010). At present, we still know little about how to distinguish the respective roles of phytoplankton and zooplankton in the pCO_2 variability. So, to evaluate the effect of biological processes on pCO_2 variability, all the biological activities were treated as a whole and suppressed in the model. In the case without any biological effect, pCO_2 was a little higher than in the standard case which exhibited a draw-down of pCO_2 by biological metabolism (Fig. 8c).

Because biological metabolism is basically a CO_2 consuming process, the net effect of biological processes was always negative and

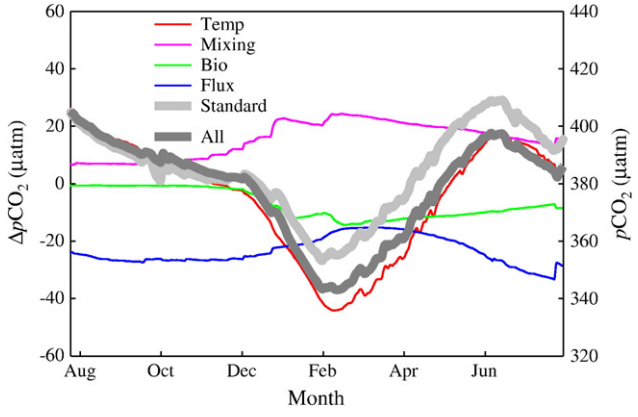

Fig. 9. The red, pink, green, and blue line show the effect of temperature (Temp), vertical mixing (Mixing), biological processes (Bio), and sea–air flux (Flux) on surface seawater pCO_2, respectively. The dark gray line reproduces the pCO_2 variation by adding the pCO_2 of the starting point with the individual pCO_2 contributions by different effecting factors together. The light gray line shows the pCO_2 variation in the standard run. (For interpretation of the references to color in this figure legend, the reader is referred to the web version of this article.)

Please cite this article as: Lu, Z., et al., Modeling seasonal and diurnal pCO_2 variations in the northern South China Sea, J. Mar. Syst. (2011), doi:10.1016/j.jmarsys.2011.10.003

ranging from −14 μatm to −1 μatm (Fig. 9). The greatest effect of the biological processes occurred in the winter with the strongest mixing and suggests that the nutrients from the deep layer were key to phytoplankton growth in the upper layer.

4.1.4. Effect of sea–air flux

Sea–air CO_2 flux is driven by the sea–air pCO_2 difference, and has strong feedback on surface water pCO_2 through the transference of CO_2 between the atmosphere and water. The effect of sea–air CO_2 exchange on the surface seawater pCO_2 was evaluated by suppressing the sea–air pCO_2 flux in the model so that there was no CO_2 exchange. The effect of the sea–air flux was stronger than the effects of vertical mixing and biological processes (Fig. 8d). pCO_2, in the case without sea–air flux, was always higher than in the standard case. However, the difference was relatively small during the winter because the seawater pCO_2 of the standard case was lower than the atmospheric pCO_2 at that time. In the NSCS, pCO_2 in seawater is higher than in the atmosphere during most of the year; the CO_2 influx in the winter only partially counteracts the accumulated CO_2 efflux from other seasons. Thus, without sea–air flux, pCO_2 is always higher than that with sea–air flux. The net effects of sea–air CO_2 exchange were always negative and varied from −33 μatm to −15 μatm (Fig. 9), since the NSCS was a weak CO_2 source to the atmosphere on an annual basis in this simulation.

When we added the entire pCO_2 offset caused by the SST, mixing, biological forcing, and sea–air flux to the pCO_2 at the beginning of the model run, we reproduced a pCO_2 that matched the standard case (Fig. 9). This indicated that separating different pCO_2-control factors/processes in these sensitivity experiments was a reasonable approach and that these factors/processes could represent the major controls of pCO_2 variation. The minor mismatch (~10 μatm) was supposedly caused by the nonlinear interaction between different processes. For example, when discussing the case without sea–air CO_2 flux, part of the elevated pCO_2 was actually due to the extra temperature-driven enhancement. In other words, the temperature effect was stronger in the case without sea–air flux and might result in an overestimation of the effect of the sea–air CO_2 flux.

4.1.5. Relative contribution

Fig. 10 shows the relative contributions of different factors/processes to surface seawater pCO_2. The percentage of each contribution was obtained by dividing the individual contribution by the sum of the contributions. The sea–air CO_2 flux was obviously the most important process that regulated the pCO_2 variation on a seasonal scale. It accounted for about 38% of year round pCO_2 variation. The contributions of temperature, vertical mixing, and biological processes to pCO_2 were 30%, 23%, and 9%, respectively. The contribution of sea–air CO_2 flux and vertical mixing on surface seawater pCO_2 has seldom been discussed in the past, however, it is generally agreed that temperature is a major regulating factor over the biological effect in this region (Chai et al., 2009; Chou et al., 2005; Zhai et al., 2005). The biological effect generally weakens from high latitude to low latitude (Takahashi et al., 2002).

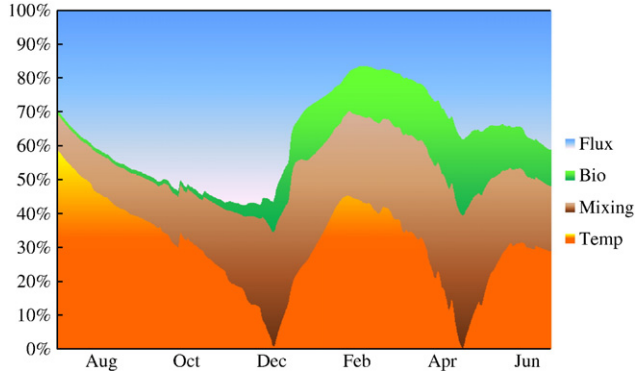

Fig. 10. The relative contributions (percentage) of different pCO_2-controlling processes to the pCO_2 variation. Flux, Bio, Mixing, and Temp represent sea–air flux, biological processes, vertical mixing, and temperature effect, respectively. Their percentages are measured by the vertical height of each component (color). The mean relative contribution of temperature, vertical mixing, biological processes, and sea–air CO_2 exchange to surface pCO_2 are 30%, 23%, 9%, and 38%, respectively. (For interpretation of the references to color in this figure legend, the reader is referred to the web version of this article.)

Due to the limitations of the model, the effect of calcium carbonate precipitation and dissolution (Eq. (15)) was not included in this numerical study.

$$Ca^{2+} + 2HCO_3^- \Leftrightarrow CaCO_3 + CO_2 + H_2O \quad (15)$$

However, its contribution to pCO_2 could be estimated from the calcification by marine organisms in the upper ocean. Based on models and observations, the global new production of $CaCO_3$ ranges from 0.8 to 1.4 Pg $CaCO_3$–C $year^{-1}$ in the euphotic zone (Feely et al., 2004). If we assume an average depth of 200 m for the euphotic zone, and assume that the calcification process were vertically uniform, and assume that the surface area of the global ocean were 3.61×10^8 km^2, we would estimate the accumulated new $CaCO_3$ production to be about 0.9–1.6 μmol $CaCO_3$ L^{-1} yr^{-1}. This would cause about a 0.9–1.6 μmol kg^{-1} decrease to DIC and about a 1.8–3.2 μmol kg^{-1} decrease to TA per year. If the average surface TA and DIC in the NSCS were 2200 μmol kg^{-1} and 1900 μmol kg^{-1}, respectively (Chai et al., 2009; Tseng et al., 2007), the decrease in TA and DIC, induced by $CaCO_3$ production, would result in a 1–2 μatm pCO_2 increase per year (using summer SST ~29 °C). Thus, on a seasonal scale, the calcification effect is relatively minor compared to the above four processes.

4.2. Surface seawater pCO_2 variability on diurnal scales

The regulation of the different processes on the surface seawater pCO_2 has different characteristics. For example, pCO_2 responds to SST variation instantly, but there is no cumulative effect. The sea–air CO_2 exchange is a slow process but it does have a cumulative effect, therefore, its contribution to pCO_2 is more significant on longer time scales such as seasonal scales. Biological processes and vertical mixing quickly change the seawater pCO_2 and their effects also accumulate. Therefore, the mechanisms and relative contributions of different pCO_2 control processes might differ on different time scales.

On diurnal scales, field observations in the open ocean of the NSCS demonstrated that temperature accounts for most of the surface seawater pCO_2 variability. The effects of biological processes and vertical mixing are relatively minor (Dai et al., 2009). However, observations under extreme conditions, such as strong winds, have seldom been reported and the insufficient temporal coverage under these conditions could lead to systematic bias in the conclusion.

The strength of vertical mixing was positively correlated with wind speed. The maximum wind occurred in December 1999 (model day 262–265), during which the variable range of surface seawater pCO_2 was within 2 μatm (Fig. 11). However, the SST varied about 0.53 °C at that time and it induced a net temperature effect on pCO_2 of about 8 μatm according to the estimation of Takahashi et al. (1993) ($\partial \ln pCO_2/\partial T$ is 4.23% $°C^{-1}$). Obviously, there were other contributors compensating for the temperature effect. By using the same method as in Section 4.1, sensitivity experiments were conducted to separate the different controls. The pCO_2 regulated by temperature was computed using Eq. (16):

$$TpCO_2 = pCO_{2start} + pCO_{2T} \quad (16)$$

where $TpCO_2$ is the pCO_2 regulated only by temperature and pCO_{2start} is the pCO_2 at the beginning of this period.

Please cite this article as: Lu, Z., et al., Modeling seasonal and diurnal pCO_2 variations in the northern South China Sea, J. Mar. Syst. (2011), doi:10.1016/j.jmarsys.2011.10.003

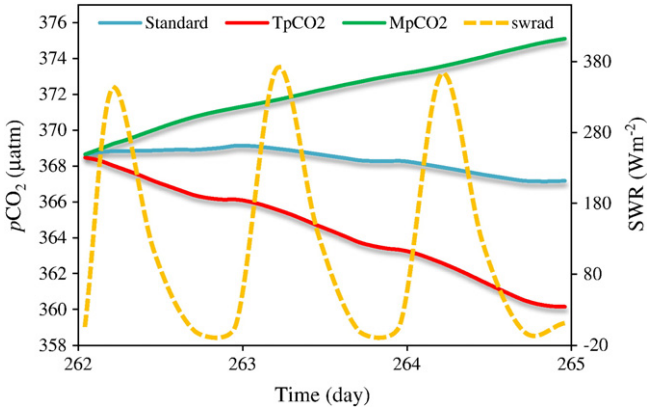

Fig. 11. The simulated pCO_2 from the standard run (blue solid line) during the maximum wind period in December 1999 (model on day 262–265, wind speed of 16–17 m s^{-1}). Also shown are the pCO_2 regulated exclusively by SST (red solid line, TpCO_2) and the pCO_2 regulated only by vertical mixing (green solid line, MpCO_2). The dark yellow dashed line shows the diurnal variation of the NCEP shortwave radiation (swrad). (For interpretation of the references to color in this figure legend, the reader is referred to the web version of this article.)

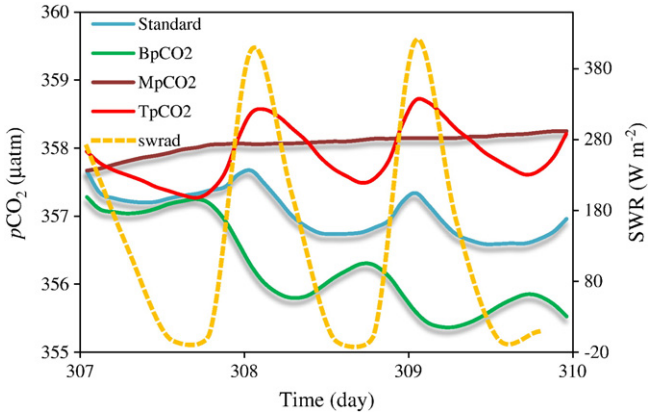

Fig. 13. The simulated pCO_2 from the standard run (blue solid line) during the maximum surface Chla period in January 2000 (model days 307–310; depth averaged Chla concentration about 0.3 µg L^{-1}). Also shown are the pCO_2 regulated only by SST (red solid line, TpCO_2), by vertical mixing (brown solid line, MpCO_2), and by biological processes (green solid line, BpCO_2). The dark yellow dashed line shows the diurnal variation of the shortwave radiation. (For interpretation of the references to color in this figure legend, the reader is referred to the web version of this article.)

The pCO_2 regulated only by vertical mixing (MpCO_2) was calculated by Eq. (17):

$$\mathrm{M}pCO_2 = pCO_{2\mathrm{start}} + \left(pCO_{2\mathrm{standard}} - pCO_{2\mathrm{mixing}}\right) \quad (17)$$

where $pCO_{2\mathrm{standard}}$ is the pCO_2 in the standard case; and $pCO_{2\mathrm{mixing}}$ is the pCO_2 of the case initialized with vertically uniform TA and DIC to remove the vertical mixing-induced chemical effect. Because Chla concentration is very low at this time and the sea–air CO_2 exchange is a relatively slow process, the effects of biological metabolism and sea–air CO_2 exchange are negligible. Fig. 11 shows that both the contributions of vertical mixing and temperature variation to pCO_2 were around 6–8 µatm. The much smaller variable range in the standard case was the result of the counterbalance between these two processes. Field data is seldom reported under this circumstance. Most field observations in the open ocean have been conducted under relatively mild wind conditions and the effect of vertical mixing has been difficult to identify. Fig. 12 further demonstrates that temperature and vertical mixing of TA and DIC were the major regulating factor/process (contribute 50% and 45% to pCO_2 variation respectively) under high wind speed.

Surface Chla reached its maximum about 7 days after the second peak of wind speed (Figs. 3a and 6) due to the time lag between phytoplankton growth and nutrient concentration increase (Gan et al., 2010). The amplitude of the simulated pCO_2 variation was within 1 µatm (Fig. 13). It had an obvious diurnal cycle which was probably caused by biological metabolism and solar radiation which are both characterized by significant diurnal variability. Again, the pCO_2 that is regulated only by temperature (TpCO_2) or vertical mixing (MpCO_2) was calculated by the same method used in the maximum wind case (Eqs. 16 and 17, respectively). The pCO_2 regulated only by biological processes was calculated by Eq. (18):

$$\mathrm{B}pCO_2 = pCO_{2\mathrm{start}} + \left(pCO_{2\mathrm{standard}} - pCO_{2\mathrm{nobio}}\right) \quad (18)$$

where $pCO_{2\mathrm{nobio}}$ is the pCO_2 for the case with all biological effects removed. Fig. 13 shows the simulated pCO_2 for the standard case and the pCO_2 evolution regulated by respective biological, temperature, and mixing forcing. The pCO_2 evolutions regulated by temperature and biological processes are qualitatively comparable to the observed data from three offshore sites reported by Dai et al. (2009), except that the observed pCO_2 had a larger variation range due to the larger diurnal amplitude of SST.

On diurnal time scales, the biological effect was more complicated than that at the seasonal time scale. Biological metabolism had negative (photosynthesis) and positive (respiration) effects on pCO_2 during the day and night respectively. On the contrary, temperature had a positive (heating) effect on seawater pCO_2 during the day and negative (cooling) effect at night. However, the pCO_2 of the standard case was out of phase with either BpCO_2 or TpCO_2 and the maximum and minimum values of pCO_2 for the standard case fall between those of BpCO_2 and TpCO_2.

These two pCO_2 controlling factors involved the following forcing processes: SST began its increase from its minimum in the early morning when the sun was rising, and, at the same time, the heat loss rate increased as SST increased. TpCO_2 reached its maximum a little later after midday and then decreased until morning. The duration of the TpCO_2 within its increasing phase was a little more than 25% of a full diurnal cycle. BpCO_2 began to decrease from its highest value in the early morning when the sun was rising due to CO_2 consumption during phytoplankton photosynthesis. This process can continue until late afternoon before sunset. Therefore, the duration of the BpCO_2 decrease was about 50% of a full diurnal cycle. The superposition of the two pCO_2 controlling processes made the maximum and minimum values of the simulated pCO_2 in the control case fall between that of BpCO_2 and TpCO_2. By removing the diurnal variation, as shown in Fig. 13, we found an increasing trend for TpCO_2 and MpCO_2 as well as a decreasing trend for BpCO_2 in the sub-diurnal frequency. Biological processes were the main controlling factors of

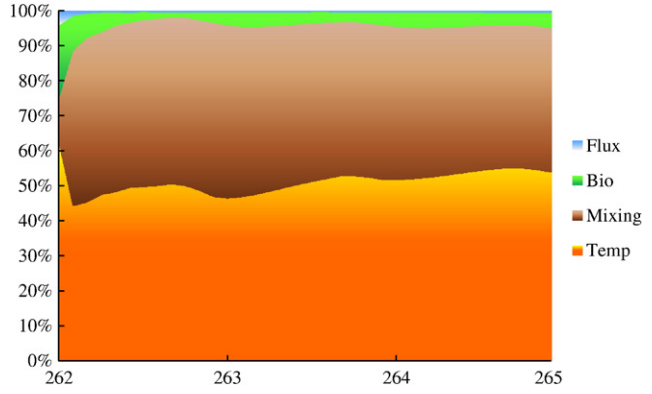

Fig. 12. Same as Fig. 10 except that this is the model run for days 262–265. The relative contribution of temperature, vertical mixing, biological process, and sea–air CO_2 exchange to surface pCO_2 are 50%, 45%, 4%, and 1% , respectively.

Please cite this article as: Lu, Z., et al., Modeling seasonal and diurnal pCO_2 variations in the northern South China Sea, J. Mar. Syst. (2011), doi:10.1016/j.jmarsys.2011.10.003

diurnal variation of pCO_2 because the pCO_2 in the standard case followed the same decreasing trend as BpCO_2. The relative contribution of the different factors is shown in Fig. 14. The average contribution of the biological processes to pCO_2 was about 60% which further proves that biological metabolism dominated the diurnal pCO_2 variation during this time.

At shorter time scales, the pCO_2 variation was closely related to changing physical and biogeochemical conditions. pCO_2 might have exhibited a similar variation pattern at different times, but its internal controlling mechanisms were very different, especially under some extreme conditions such as strong winds. The lack of field measurements during this period might have caused our study to overlook the full spectrum of the pCO_2 forcing function and might have led to considerable bias in pCO_2 variability.

We also noticed that the sea–air flux had only minor effect on pCO_2 at diurnal scales, although it was the most important controlling factor at seasonal scales. This was because of the buffering effect of the seawater carbonate system as indicated by the Revelle factor (RF, Eq. (19)) (Zeebe and Wolf-Gladrow, 2005),

$$\mathrm{RF} = \frac{\partial[CO_2]}{\partial[DIC]} \Big/ \frac{[CO_2]}{[DIC]} \tag{19}$$

which made the equilibrium of sea–air CO_2 exchange a very slow process (Murnane et al., 1999; Najjar, 1992). The CO_2 flux from atmosphere to seawater reacts with H_2O to form H_2CO_3 through hydration, and subsequently forms HCO_3^- and CO_3^{2-} ions through dissociation until it reaches equilibrium with the seawater carbonate system. Therefore seawater can contain more CO_2 than the nonreactive gasses, and the equilibration time is prolonged accordingly. If we assume an atmospheric pCO_2, mixed layer DIC concentration, and RF of 370 μatm, 2000 μmol kg^{-1} and 9, respectively (typical value of the region), and we use a water temperature of 28 °C and wind speed of 6.5 m s^{-1} (the average value during the modeling period), then the equilibration time of CO_2 in the mixed layer (50 m depth is assumed), with respect to the sea–air flux, would be about 300 days. This is the reason why the regulation of sea–air CO_2 flux on surface water pCO_2 was much more significant at seasonal scales than at diurnal scales. Discussing the sea–air CO_2 exchange and its impact on surface water pCO_2 without properly consideration of the buffering effect will lead to considerable deviation.

4.3. The long-term impact of high-frequency signals

In this study, high-frequency (6-hourly) NCEP data were used to force the model, and, as discussed in Section 4.2, significant variations of surface water pCO_2 and other variables were found to exist at diurnal time scales. pCO_2 variations at different times or under different environmental conditions were quite distinct. The long-term effects of high-frequency forcing on the variational trend of surface water pCO_2 or the sea–air CO_2 flux have been seldom reported.

We conducted three experiments with atmospheric forcing that were smoothed by a 36-hour filter to remove the diurnal signal, a 7-day filter to remove the synoptic signal, and a 30-day filter to remove the monthly signal. We compared the results from these experiments with the result from the standard run, and obtained the effects of the high-frequency forcing on physical and biogeochemical variables at longer time scales (Fig. 15).

The seasonal variations of the pCO_2 anomalies clearly showed the regulation of pCO_2 by high-frequency forcing. Positive or negative effects of up to ~30 μatm (~8% of the surface water pCO_2) alternately changed the pCO_2 variation (Fig. 15a). The lower frequency forcing (by removing signals in the higher frequency) tended to contribute to larger anomalies. The SST anomalies were positive nearly all the time (Fig. 15b) after removing the high-frequency forcing due to the reduction of turbulent kinetic energy imparted into the sea surface and thus the decreases in the latent heat flux and vertical mixing. High SST induced a positive feedback to the surface pCO_2. Similarly, without the high-frequency signals, the nutrient flux from the deep layer to the surface layer was weakened. As a consequence, Chla concentrations declined along with a lessened drawdown of CO_2 by biological consumption (Fig. 15c), which represented a positive feedback to the surface pCO_2. However, the weakened vertical mixing (indicated by the negative salinity anomaly (Fig. 15d)) also reduced the upward flux of high pCO_2 subsurface water, which was a negative feedback to the surface water pCO_2. The pCO_2 anomalies were, therefore, a composite result of those processes. The high-frequency forcing was important in controlling the pCO_2 variation at a longer time scale through the feedback effect to the corresponding physical and biogeochemical responses. Ignoring the contribution from the high-frequency forcing might introduce considerable error to the pCO_2 estimation, and might systematically overestimate or underestimate the contributions of certain pCO_2 control factors or processes.

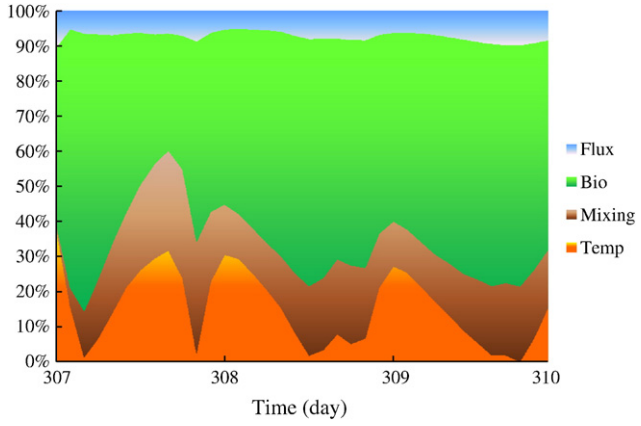

Fig. 14. Same as Fig. 10 except that these are model days 307–310. The relative contribution of temperature, vertical mixing, biological processes, and sea–air CO_2 exchange is 15%, 18%, 60%, and 7%, respectively.

5. Summary

Using a 1-D coupled physical–biogeochemical model, we analyzed the controlling mechanisms of the surface seawater pCO_2 in the NSCS at seasonal and diurnal time scales. Forced by high-frequency, time-dependent atmospheric forcing and initialized with observed physical and biogeochemical parameters, the model reproduced the observed seasonal variation of a suite of physical and biogeochemical variables reasonably well, and it confirmed that the NSCS is a sink for the atmospheric CO_2 in the winter and a source during other seasons.

Sensitivity experiments were conducted to investigate the controlling mechanisms of surface seawater pCO_2 and the relative contribution of different factors and processes to pCO_2 variability. The results indicated that the contributions were time scale dependent. At seasonal scales, the sea–air CO_2 exchange could exceed the temperature effect and act as the most important regulatory factor to the surface seawater pCO_2, even though the phase of the surface pCO_2 seasonal variation generally followed the seasonal cycle of SST. This was because the CO_2 sea–air flux has an accumulative effect on pCO_2 and tends to be a more important contributor at a longer time scale, such as at seasonal scales. Biological processes had a relatively minor effect on the pCO_2 seasonal variability.

At diurnal time scales, the dominant pCO_2 controlling factor was dependent on the local physical and biogeochemical conditions. During a strong northeasterly monsoon in winter, processes induced by intensified wind stress made a major contribution to the surface seawater pCO_2. Vertical mixing pumped the high potential pCO_2 deep water upward while intensified vertical mixing and cooling effects

Please cite this article as: Lu, Z., et al., Modeling seasonal and diurnal pCO_2 variations in the northern South China Sea, J. Mar. Syst. (2011), doi:10.1016/j.jmarsys.2011.10.003

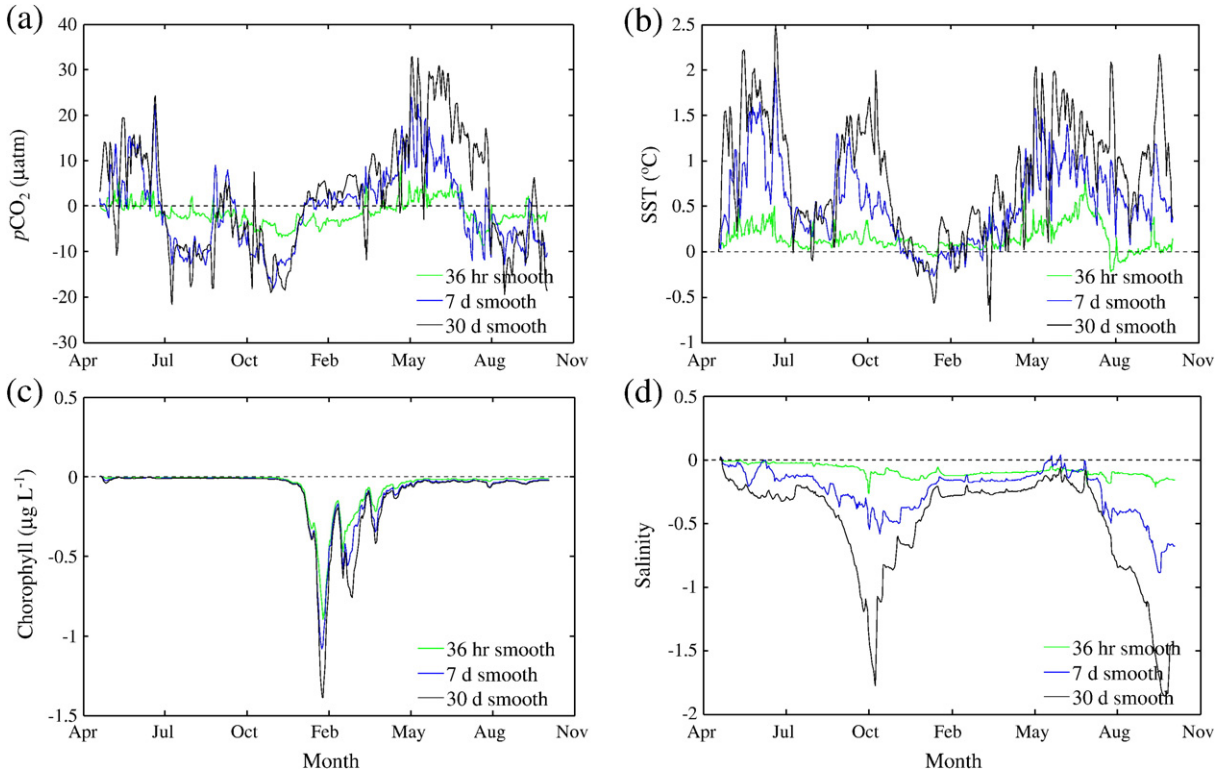

Fig. 15. Seasonal variation of pCO_2, temperature, Chla, and salinity anomalies. The anomalies of all the variables are calculated by subtracting the value of the standard run from the sensitivity cases which were forced by smoothed NCEP data.

under the strong winter monsoon decreased the SST, and then decreased the pCO_2. Nevertheless, the upward transport of high pCO_2 deep water and the cooling effect during the intensified mixing tended to offset each other, which lead to a relatively weak pCO_2 variation. Subsequently, phytoplankton blooms could occur as a result of increased nutrient concentration in the upper layer and biological metabolism would dominate the variation of surface pCO_2. It formed a significant diurnal pCO_2 cycle due to a composite effect of the diurnal cycle of solar radiation and phytoplankton metabolism. Sea–air CO_2 flux had a minor effect on surface seawater pCO_2 at diurnal time scales because CO_2 sea–air equilibration is a relatively slow process due to the buffering effect of the seawater carbonate systems. It generally takes about 1 year for CO_2 in the atmosphere and mixed layer in the ocean to reach equilibrium.

The surface water pCO_2 and CO_2 sea–air flux were very sensitive to the temporal variation in atmospheric forcing. The discrepancy between pCO_2 forced with monthly and higher frequency atmospheric forcing can be as great as 30 μatm. Systematically overestimated or underestimated pCO_2 and sea–air CO_2 fluxes would be produced if the high frequency signals were ignored.

Acknowledgments

The authors appreciate the help provided by Y. Cheung for assistance in modeling and data processing. This research was supported by the National Key Basic Research Development Program under projects 2009CB421208 and 2009CB421201; and by HKUST research project RCP10IPO01.

Appendix A

The Regional Ocean Modeling System (ROMS) that we used in this study is version 3.0. In this version, some settings/functions were not suitable for this application; therefore, revisions were made as listed below:

The TA was treated as a diagnostic variable and was a function of salinity (Brewer et al., 1986) in the original set up.

$$[TA] = 587.05 + 50.56 \times \text{Salinity} \quad \text{(A1)}$$

In this study, TA was initialized with observed data, so the diagnostic calculation of TA was inhibited.

In the original model, CO_2 solubility was calculated according to Eq. (A2) according to the formula in Weiss (1974), the resulting unit is "mol kg^{-1} atm^{-1}".

$$CO_{2sol} = \exp(-60.2409 + 93.4517/T_K + 23.3585 \times \log(T_K) + \text{Salinity} \times (0.023517 + T_K \times (-0.023656 + 0.0047036 \times T_K))) \quad \text{(A2)}$$

where, CO_2_sol represents CO_2 solubility, and T_K is the absolute temperature ($T_K = T + 273.15$).

However, CO_2 solubility should appear with units of "mol L^{-1} atm^{-1}" when calculating the sea–air CO_2 flux to derive the correct units for flux. Therefore, Eq. (A3) was used to calculate CO_2 solubility in this study.

$$CO_{2sol} = \rho \times exp(-60.2409 + 93.4517/T_K + 23.3585 \times \log(T_K) + \text{Salinity} \times (0.023517 + T_K \times (-0.023656 + 0.0047036 \times T_K))) \quad \text{(A3)}$$

where, ρ represents seawater density in unit of kg L^{-1}.

When calculating the sea–air CO_2 flux (F_{CO2}) using Eq. (12), the sea–air pCO_2 difference was calculated by:

$$\Delta pCO_2 = pCO_{2air} - pCO_{2water} \quad \text{(A4)}$$

Please cite this article as: Lu, Z., et al., Modeling seasonal and diurnal pCO_2 variations in the northern South China Sea, J. Mar. Syst. (2011), doi:10.1016/j.jmarsys.2011.10.003

where pCO_{2air} represents the atmospheric pCO_2 in the marine boundary layer, and pCO_{2water} represents the surface seawater pCO_2. The pCO_{2air} in the original program simulated the monthly variation using Eq. (A5):

$$\begin{aligned} pCO_{2air}\text{secular} = {} & 282.6 + 0.125 \times \text{pmonth} \times 12 - 7.18 \\ & \times \sin(\text{pi2} \times \text{pmonth} + 0.86) - 0.99 \\ & \times \sin(\text{pi2} \times \text{pmonth} + 0.28) - 0.80 \\ & \times \sin(\text{pi2} \times \text{pmonth} + 0.06) \end{aligned} \quad \text{(A5)}$$

where $pCO_{2air_}$secular represents the secular monthly pCO_{2air}; pmonth represents the months since Jan 1951; and pi2 is a constant equal to 6.2831853071796.

The sea–air CO_2 flux was produced as an accumulated term in the original program. In other words, F_{CO2} was the time-integrated CO_2 sea–air flux (total amount). In this study, the corresponding code was revised to produce the real-time CO_2 flux (rate).

References

Bates, N.R., Takahashi, T., Chipman, D.W., Knap, A.H., 1998. Variability of pCO_2 on diel to seasonal timescales in the Sargasso Sea near Bermuda. Journal of Geophysical Research-Oceans 103 (C8), 15567–15585.

Brewer, P.G., Bradshaw, A.L., Williams, R.T., 1986. Measurements of total carbon dioxide and alkalinity in the North Atlantic Ocean in 1981. In: Trabalka, J.R., Reichle, D.E. (Eds.), The Changing Carbon Cycle: A Global Analysis. Springer, New York, pp. 348–370.

Cai, W.J., Dai, M.H., Wang, Y.C., 2006. Air–sea exchange of carbon dioxide in ocean margins: a province-based synthesis. Geophysical Research Letters 33 (12), L12603 Doi: 12610.11029/12006GL026219.

Chai, F., Liu, G.M., Xue, H.J., Shi, L., Chao, Y., Tseng, C.M., Chou, W.C., Liu, K.K., 2009. Seasonal and interannual variability of carbon cycle in South China Sea: a three-dimensional physical–biogeochemical modeling study. Journal of Oceanography 65 (5), 703–720.

Chen, Y.F.L., 2005. Spatial and seasonal variations of nitrate-based new production and primary production in the South China Sea. Deep-Sea Research I 52 (2), 319–340.

Chou, W.C., Sheu, D.D.D., Chen, C.T.A., Wang, S.L., Tseng, C.M., 2005. Seasonal variability of carbon chemistry at the SEATS time-series site, northern South China Sea between 2002 and 2003. Terrestrial Atmospheric and Oceanic Sciences 16 (2), 445–465.

Dai, M.H., Lu, Z.M., Zhai, W.D., Chen, B.S., Cao, Z.M., Zhou, K.B., Cai, W.J., Chen, C.T.A., 2009. Diurnal variations of surface seawater pCO_2 in contrasting coastal environments. Limnology and Oceanography 54 (3), 735–745.

Evans, G.T., Garcon, V.C., 1997. One-Dimensional Models of Water Column Biogeochemistry. Report. 23/97. Bergen, Norway. 85 pp,.

Falkowski, P., Scholes, R.J., Boyle, E., Canadell, J., Canfield, D., Elser, J., Gruber, N., Hibbard, K., Hogberg, P., Linder, S., Mackenzie, F.T., Moore, B., Pedersen, T., Rosenthal, Y., Seitzinger, S., Smetacek, V., Steffen, W., 2000. The global carbon cycle: a test of our knowledge of earth as a system. Science 290 (5490), 291–296.

Fasham, M.J.R., Ducklow, H.W., McKelvie, S.M., 1990. A nitrogen-based model of plankton dynamics in the oceanic mixed layer. Journal of Marine Research 48, 591–639.

Feely, R.A., Sabine, C.L., Lee, K., Berelson, W., Kleypas, J., Fabry, V.J., Millero, F.J., 2004. Impact of anthropogenic CO_2 on the $CaCO_3$ system in the oceans. Science 305 (5682), 362–366.

Fennel, K., Wilkin, J., Levin, J., Moisan, J., O'Reilly, J., Haidvogel, D., 2006. Nitrogen cycling in the Middle Atlantic Bight: results from a three-dimensional model and implications for the North Atlantic nitrogen budget. Global Biogeochemical Cycles 20 (3) GB3007, doi 3010.1029/2005GB002456.

Fujii, M., Chai, F., Shi, L., Inoue, H.Y., Ishii, M., 2009. Seasonal and interannual variability of oceanic carbon cycling in the western and central tropical–subtropical Pacific: a physical–biogeochemical modeling study. Journal of Oceanography 65 (5), 689–701.

Gan, J., Lu, Z.M., Dai, M.H., Cheung, A., Harrison, P., Liu, H.B., 2010. Biological response to intensified upwelling and to a river plume in the northeastern South China Sea: a modeling study. Journal of Geophysical Research-Oceans 115, C09001 doi:09010.01029/02009JC005569.

Haidvogel, D.B., Arango, H., Budgell, W.P., Cornuelle, B.D., Curchitser, E., Di Lorenzo, E., Fennel, K., Geyer, W.R., Hermann, A.J., Lanerolle, L., Levin, J., McWilliams, J.C., Miller, A.J., Moore, A.M., Powell, T.M., Shchepetkin, A.F., Sherwood, C.R., Signell, R.P., Warner, J.C., Wilkin, J., 2008. Ocean forecasting in terrain-following coordinates: formulation and skill assessment of the Regional Ocean Modeling System. Journal of Computational Physics 227 (7), 3595–3624.

Keeling, R.F., 2008. Atmospheric science — recording Earth's vital signs. Science 319 (5871), 1771–1772.

Liu, H.B., Chen, M.R., Suzuki, K., Wong, C.K., Chen, B.Z., 2010. Mesozooplankton selective feeding in subtropical coastal waters as revealed by HPLC pigment analysis. Marine Ecology Progress Series 407, 111–123.

Liu, K.K., Chao, S.Y., Shaw, P.T., Gong, G.C., Chen, C.C., Tang, T.Y., 2002. Monsoon-forced chlorophyll distribution and primary production in the South China Sea: observations and a numerical study. Deep-Sea Research I 49 (8), 1387–1412.

Liu, K.K., Kao, S.J., Hu, H.C., Chou, W.C., Hung, G.W., Tseng, C.M., 2007. Carbon isotopic composition of suspended and sinking particulate organic matter in the northern South China Sea — from production to deposition. Deep-Sea Research II 54 (14–15), 1504–1527.

Louanchi, F., Metzl, N., Poisson, A., 1996. Modelling the monthly sea surface fCO_2 fields in the Indian Ocean. Marine Chemistry 55 (3–4), 265–279.

Lu, Z.M., Gan, J.P., Dai, M.H., Cheung, A.Y.Y., 2010. The influence of coastal upwelling and a river plume on the subsurface chlorophyll maximum over the shelf of the northeastern South China Sea. Journal of Marine Systems 82 (1–2), 35–46. doi:10.1016/j.jmarsys.2010.1003.1002.

McKinley, G.A., Takahashi, T., Buitenhuis, E., Chai, F., Christian, J.R., Doney, S.C., Jiang, M.S., Lindsay, K., Moore, J.K., Le Quere, C., Lima, I., Murtugudde, R., Shi, L., Wetzel, P., 2006. North Pacific carbon cycle response to climate variability on seasonal to decadal timescales. Journal of Geophysical Research-Oceans 111 (C7). doi:10.1029/2005JC003173 C07S06.

Mellor, G.L., Yamada, T., 1982. Development of a turbulence closure-model for geophysical fluid problems. Reviews of Geophysics 20 (4), 851–875.

Murnane, R.J., Sarmiento, J.L., Le Quere, C., 1999. Spatial distribution of air–sea CO_2 fluxes and the interhemispheric transport of carbon by the oceans. Global Biogeochemical Cycles 13 (2), 287–305.

Najjar, R.G., 1992. Marine biogeochemistry. Climate System Modeling, edited by K. E. Trenberth. Cambridge Univ. Press, New York, pp. 241–280.

Previdi, M., Fennel, K., Wilkin, J., Haidvogel, D., 2009. Interannual variability in atmospheric CO_2 uptake on the northeast US continental shelf. Journal of Geophysical Research-Biogeosciences 114. doi:10.1029/2008JG000881.

Redfield, A.C., 1958. The biological control of chemical factors in the environment. American Scientist 46, 205–211.

Shchepetkin, A.F., McWilliams, J.C., 2005. The regional oceanic modeling system (ROMS): a split-explicit, free-surface, topography-following-coordinate oceanic model. Ocean Modelling 9 (4), 347–404.

Swapna, P., Gan, J.P., Lau, A., Fung, J., 2009. On the warm/cold regime shift in the South China Sea: observation and modeling study. Deep Sea Research I 56 (7), 1039–1056 1010.1016/j.dsr.2009.1003.1008.0.

Takahashi, T., Olafsson, J., Goddard, J.G., Chipman, D.W., Sutherland, S.C., 1993. Seasonal variation of CO_2 and nutrients in the high-latitude surface oceans: a comparative study. Global Biogeochemical Cycles 7, 843–878.

Takahashi, T., Sutherland, S.C., Sweeney, C., Poisson, A., Metzl, N., Tilbrook, B., Bates, N., Wanninkhof, R., Feely, R.A., Sabine, C., Olafsson, J., Nojiri, Y., 2002. Global sea–air CO_2 flux based on climatological surface ocean pCO_2, and seasonal biological and temperature effects. Deep-Sea Research II 49 (9–10), 1601–1622.

Takahashi, T., Sutherland, S.C., Wanninkhof, R., Sweeney, C., Feely, R.A., Chipman, D.W., Hales, B., Friederich, G., Chavez, F., Sabine, C., Watson, A., Bakker, D.C.E., Schuster, U., Metzl, N., Yoshikawa-Inoue, H., Ishii, M., Midorikawa, T., Nojiri, Y., Kortzinger, A., Steinhoff, T., Hoppema, M., Olafsson, J., Arnarson, T.S., Tilbrook, B., Johannessen, T., Olsen, A., Bellerby, R., Wong, C.S., Delille, B., Bates, N.R., de Baar, H.J.W., 2009. Climatological mean and decadal change in surface ocean pCO_2, and net sea–air CO_2 flux over the global oceans. Deep-Sea Research Part II 56 (8–10), 554–577.

Tseng, C.M., Wong, G.T.F., Lin, I.I., Wu, C.R., Liu, K.K., 2005. A unique seasonal pattern in phytoplankton biomass in low-latitude waters in the South China Sea. Geophysical Research Letters 32 (8). doi:10.1029/2004GL022111.

Tseng, C.M., Wong, G.T.F., Chou, W.C., Lee, B.S., Sheu, D.D., Liu, K.K., 2007. Temporal variations in the carbonate system in the upper layer at the SEATS station. Deep-Sea Research II 54 (14–15), 1448–1468.

Wanninkhof, R., 1992. Relationship between wind-speed and gas-exchange over the ocean. Journal of Geophysical Research-Oceans 97 (C5), 7373–7382.

Weiss, R.F., 1974. Carbon dioxide in water and seawater: the solubility of a non-ideal gas. Marine Chemistry 2, 203–215.

Wong, G.T.F., Ku, T.L., Mulholland, M., Tseng, C.M., Wang, D.P., 2007. The SouthEast Asian time-series study (SEATS) and the biogeochemistry of the South China Sea — an overview. Deep-Sea Research II 54 (14–15), 1434–1447.

Zeebe, R.E., Wolf-Gladrow, D., 2005. CO_2 in Seawater: Equilibrium, kinetics, isotopes. Elsevier Science B. V, Amsterdam. 346 pp,.

Zhai, W.D., Dai, M.H., 2009. On the seasonal variation of air–sea CO_2 fluxes in the outer Changjiang (Yangtze River) Estuary, East China Sea. Marine Chemistry 117 (1–4), 2–10.

Zhai, W.D., Dai, M.H., Cai, W.J., Wang, Y.C., Hong, H.S., 2005. The partial pressure of carbon dioxide and air–sea fluxes in the northern South China Sea in spring, summer and autumn. Marine Chemistry 96 (1–2), 87–97.

Zhai, W.D., Dai, M.H., Cai, W.J., Wang, Y.C., Hong, H.S., 2007. Erratum to "The partial pressure of carbon dioxide and air–sea fluxes in the northern South China Sea in spring, summer and autumn"[Marine Chemistry 96 (2005) 87–97]. Marine Chemistry 103 (1–2), 209.

Please cite this article as: Lu, Z., et al., Modeling seasonal and diurnal pCO_2 variations in the northern South China Sea, J. Mar. Syst. (2011), doi:10.1016/j.jmarsys.2011.10.003